Original Article

Prediction of Kirsten rat sarcoma (*KRAS*) mutation in rectal cancer with amide proton transfer-weighted magnetic resonance imaging

Xinyue Yang[1#], Qing Qiu[2#], Weirong Lu[3], Bingmei Chen[1], Minning Zhao[1], Wen Liang[1], Zhibo Wen[1]

[1]Department of Radiology, Zhujiang Hospital, Southern Medical University, Guangzhou, China; [2]Department of Radiology, Guangdong Provincial People's Hospital (Guangdong Academy of Medical Sciences), Southern Medical University, Guangzhou, China; [3]Department of Medical Imaging Center, Nanfang Hospital, Southern Medical University, Guangzhou, China

Contributions: (I) Conception and design: X Yang, Z Wen; (II) Administrative support: W Liang, Z Wen; (III) Provision of study materials or patients: W Liang, Z Wen; (IV) Collection and assembly of data: Q Qiu, W Lu, B Chen, M Zhao; (V) Data analysis and interpretation: X Yang, Q Qiu; (VI) Manuscript writing: All authors; (VII) Final approval of manuscript: All authors.

[#]These authors contributed equally to this work.

Correspondence to: Zhibo Wen, MD, PhD. Department of Radiology, Zhujiang Hospital, Southern Medical University, 235 Gongye Avenue Middle, Haizhu District, Guangzhou 510280, China. Email: zhibowen@163.com.

Background: Kirsten rat sarcoma (*KRAS*) mutation drives resistance to anti-epidermal growth factor receptor (anti-EGFR)-targeted therapies in rectal cancer. Amide proton transfer-weighted magnetic resonance imaging (APTw MRI) might be a supplement to the evaluation of *KRAS* mutation because the APTw value can reflect mobile cellular protein content *in vivo*. This study aimed to determine whether APTw MRI could predict *KRAS* mutation in rectal cancer and compare this technique with diffusion-weighted imaging (DWI).

Methods: This retrospective study reviewed 153 consecutive patients with rectal cancer from April 2019 to June 2021 in our hospital. Among them, a total of 55 patients who did not undergo neoadjuvant chemoradiotherapy and underwent preoperative APTw MRI, DWI, and postoperative *KRAS* tests were included in this study. In two-dimensional APTw images, two radiologists manually delineated three regions of interest (ROIs) along tumor contour in the largest slice and the adjacent two slices of tumor respectively. The mean APTw value within a ROI was calculated, and the values of three ROIs were averaged for each patient. In consecutive DWI images, two radiologists depicted the ROIs of the whole lesion, and the mean apparent diffusion coefficient (ADC) was generated. The intraclass correlation coefficient (ICC), Shapiro-Wilk test and Student's *t*-test were used for statistical analyses. Receiver operating characteristic (ROC) curves were constructed for APTw and ADC values respectively, and the area under the curve (AUC) was used to evaluate the diagnostic performance for the prediction of *KRAS* mutation.

Results: Among these 55 patients, *KRAS* mutation occurred in 21 patients. The ICCs of two independent raters for APTw and ADC values were 0.937 [95% confidence interval (CI), 0.914–0.953] and 0.976 (95% CI, 0.959–0.986), respectively. ADC values did not show a statistically significant difference between the *KRAS*-mutant group and the wild type (WT) group (P=0.733). *KRAS*-mutant tumors exhibited a higher APTw value than WT tumors in patients with rectal non-mucinous adenocarcinoma (3.324%±0.685% *vs.* 2.230%±0.833%, P<0.001). The AUC of the APTw value was 0.827 (95% CI, 0.701–0.916), with a cutoff value of 2.4% (sensitivity, 95.2%; specificity, 55.9%).

Conclusions: DWI cannot differentiate mutant *KRAS* genes from WT genes in patients with rectal cancer, but APTw MRI has potential for evaluating *KRAS* mutation in rectal cancer. The APTw value had moderate diagnostic performance in the prediction of *KRAS* mutation with a high sensitivity but a low specificity. APTw MRI might be a promising supplement to *KRAS* genomic analysis in rectal cancer patients.

Keywords: Rectal cancer; Kirsten rat sarcoma (*KRAS*); diffusion-weighted imaging (DWI); amide proton transfer (APT); magnetic resonance imaging (MRI)

Submitted Feb 20, 2024. Accepted for publication Aug 02, 2024. Published online Sep 04, 2024.
doi: 10.21037/qims-24-331
View this article at: https://dx.doi.org/10.21037/qims-24-331

Introduction

Colorectal cancer (CRC) is the third most common neoplasm worldwide (1). The Kirsten rat sarcoma (*KRAS*) gene plays an important role in the treatment and prognosis of CRC patients. About 40% of CRC patients have *KRAS* mutations (2). This mutation drives primary resistance to the epidermal growth factor receptor (EGFR) antibody-targeted therapies, such as cetuximab and panitumumab (2). Besides, *KRAS* mutation indicates a poor prognosis and a worse response to neoadjuvant chemoradiotherapy in patients with locally advanced rectal cancer (3). Thus, *KRAS* testing has been recommended for all metastatic CRC patients, and is mandatory before anti-EGFR-targeted therapies (2).

Although DNA sequencing is universally acknowledged as the gold standard for *KRAS* mutation testing, the sensitivity of this complex and time-consuming method is extremely low, at about 10–30% (2). Polymerase chain reaction (PCR)-based testing methods predominate in mutational analysis because of their current effectiveness and availability (2). However, *KRAS* status can be heterogeneous within a primary colorectal tumor, leading to an inaccurate histological testing result (4). Moreover, false-positive *KRAS* mutation testing results are linked to other factors such as the DNA fragmentation caused by improper fixation and the influence of stromal cells (4). Thus, a non-invasive and convenient way of evaluating *KRAS* mutation facilitate the personal treatment strategy for each patient with rectal cancer.

Magnetic resonance imaging (MRI) has been recommend for patients with rectal cancer before treatment in the National Comprehensive Cancer Network (NCCN) guidelines (5). The functional sequence, diffusion-weighted imaging (DWI), could non-invasively quantify water diffusion in *in vivo* tissue (6). DWI has been widely applied in clinical practice. Some previous studies has used apparent diffusion coefficient (ADC) derived from DWI to evaluate *KRAS* mutation in rectal cancer, but their results still remain controversial (7-10).

Generally, *KRAS* mutation will result in KRAS proteins accumulate in cells (4). In order to non-invasively detect cellular protein content, a molecular MRI named amide proton transfer-weighted (APTw) MRI was proposed (11). APTw MRI generates image contrast predominantly based on amide protons in endogenous mobile cellular proteins and peptides within *in vivo* tissue (11). Several clinical studies that apply APTw MRI to tumors have been reported, suggesting that this technique has remarkable promise (12-15). In rectal cancer research, APTw MRI has been used to evaluate tumor grade and pathological prognostic factors, assess p53 and Ki-67 expression, and predict tumor response to neoadjuvant chemotherapy (16-19). However, few studies have focused on the relationship between APTw signals and *KRAS* status in rectal cancer.

Therefore, this study aimed to determine whether APTw MRI can differentiate mutant *KRAS* genes from WT genes in patients with rectal cancer and investigate its utility in predicting *KRAS* mutation, in comparison with DWI. We present this article in accordance with the STARD reporting checklist (available at https://qims.amegroups.com/article/view/10.21037/qims-24-331/rc).

Methods

Patients

This retrospective study was conducted in accordance with the Declaration of Helsinki (as revised in 2013). It was approved by the Institutional Review Board of Zhujiang Hospital and complied with the standards of the Ethical Committee (No. 2020-KY-029-01). The requirement for patient informed consent was waived. From April 2019 to June 2021, 153 patients with biopsy-confirmed rectal adenocarcinoma located within 15 centimeters from the anal verge were reviewed. Patients who underwent neoadjuvant chemoradiotherapy, did not undergo preoperative APTw MRI, DWI, or total mesorectal excision in our hospital, or had a mucinous tumor or composition of mucinous adenocarcinoma were excluded. Patients who did not undergo postoperative *KRAS* testing were also excluded. We also excluded 11 cases due to poor APTw image quality caused by motion or metal artifacts. Eventually, a total of 55 patients

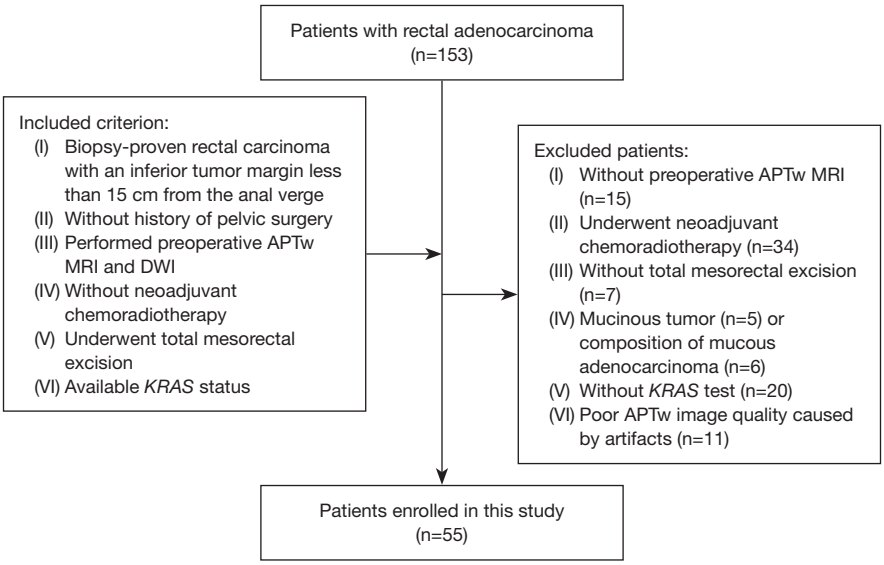

Figure 1 The flowchart of the patients in this study. APTw, amide proton transfer-weighted; MRI, magnetic resonance imaging; DWI, diffusion-weighted imaging; *KRAS*, Kirsten rat sarcoma.

were enrolled in this study (*Figure 1*). The mean interval between MRI examination and operation was 3.67 days (range, 0–8 days).

MRI protocol

MRI examination was performed using a 3.0-Tesla MR system (Ingenia; Philips Healthcare, Best, the Netherlands) with a 32-channel phased-array torso coil. An appropriate amount of ultrasound gel was administrated to each patient in order to prevent image structure distortion. To reduce bowel peristalsis, 10 mg of raceanisodamine hydrochloride was injected intramuscularly 10 minutes before the MRI examination unless contraindicated. Sagittal, coronal, oblique axial T2-weighted (T2W) images, and oblique axial contrast-enhanced T1-weighted images were obtained by using turbo spin echo (TSE) sequences. Before gadodiamide (Omniscan; GE Healthcare, Dublin, Ireland) injection, raw data of APTw MRI were acquired with a fat suppression two-dimensional TSE-Dixon pulse sequence. Quasi-continuous saturation prepulse with the power of 2 μT and duration of 1 second was enabled by using two transmission channels in alternation during APT saturation. A total of 19 saturation frequency offsets (one at –1,540 ppm, ±3.5 ppm and 16 around them with a step size of 0.8 ppm) were acquired and corrected with intrinsic B_0 map of TSE-Dixon scanning. The image acquired at –1,540 ppm was used for signal normalization. The SENSE factor of APT sequence was 1.3. The saturation pulse was composed of 20 elements with a duration of 50 ms and sinc-Guassian shape. The largest slice of tumor and the adjacent two slices were select to obtain tumor oblique axial images of Z-spectrum series by referring to the sagittal, coronal, and oblique axial T2W images. DWI with *b* values of 0 and 1,000 s/mm^2 was also performed before the injection of contrast agent by using single-shot echo-planar imaging (SS-EPI). The other parameters of the MRI protocol are detailed in *Table 1*.

Image analysis

The APTw images were calculated by using the software MATLAB (MathWorks, Natick, MA, USA) according to the equation below:

$$MTR_{asym} = \left(S_{-\Delta\omega} - S_{\Delta\omega}\right)/S_0 \quad [1]$$

where MTR_{asym} is magnetization transfer ratio asymmetry, $S_{-\Delta\omega}$ is B_0 corrected signal at –3.5 ppm, $S_{\Delta\omega}$ is B_0 corrected signal at 3.5 ppm, and S_0 is the normalization factor acquired at –1,540 ppm. It is appropriate to define the calculated MTR_{asym} (3.5 ppm) images as APTw images. The APTw value was defined as MTR_{asym} (3.5 ppm) multiplied by 100%.

The ADC maps were generated by the software Medical Imaging Interaction Toolkit (MITK, https://www.mitk.org)

Table 1 MRI protocol for rectal cancer

Parameters	Sagittal T2WI	Coronal T2WI	Oblique axial T2WI	DWI (b=0, 1,000 s/mm^2)	APTw imaging	Contrast-enhanced oblique axial T1WI
Sequence	TSE	TSE	TSE	EPI	TSE	TSE
TR (ms)	3,604	3,000	3,000	6,000	2,762	574
TE (ms)	100	80	80	61	4.9	8
ETL	21	21	21	59	16	8
NEX	2	2	2	2	1	1
Slices	24	24	24	18	3	24
Slice thickness (mm)	3	3	3	4	5	3
Slice gap (mm)	0.3	0.3	0.3	0.4	0.5	0.3
FOV (mm)	240×198	220×220	332×293	200×249	212×191	200×200
Voxel size (mm)	0.80×0.79×3.00	0.80×0.80×3.00	0.60×0.61×3.00	2.50×2.09×4.00	2.50×2.51×5.00	0.90×1.00×3.00
Acquisition matrix	300×234	276×230	332×293	80×118	84×73	224×196
Fat suppression	N/A	N/A	N/A	SPAIR	SPIR	SPIR
Flip angle (deg)	90	90	90	90	90	90
Scan time (min:s)	03:04	02:12	03:00	02:06	05:23	02:01

MRI, magnetic resonance imaging; T2WI, T2-weighted imaging; DWI, diffusion-weighted imaging; APTw, amide proton transfer-weighted; T1WI, T1-weighted imaging; TSE, turbo spin echo; EPI, echo-planar imaging; TR, repetition time; TE, echo time; ETL, echo train length; NEX, number of excitations; FOV, field of view; N/A, not applicable; SPAIR, spectral attenuated inversion recovery; SPIR, spectral pre-saturation with inversion recovery.

based on the following equation:

$$S_b/S_0 = \exp(-bADC) \quad [2]$$

Where S_b and S_0 are the signal intensity at b values of 1,000 and 0 s/mm^2 respectively, and the b value is 1,000 s/mm^2.

Two radiologists (with 7 and 4 years of respective experience interpreting rectal MR images) who were blind to pathological findings used the software Image J (National Institutes of Health, Bethesda, MD, USA) to measure the tumor APTw values respectively. Referring to T2W images, a region of interest (ROI) was manually drawn on the representative image of Z-spectrum series which showed the tumor of each slice most clearly, covering most of tumor parenchyma and excluding visible cystic, necrotic, or hemorrhagic components. Then, these ROIs of three slices were copied to corresponding APTw images. The mean APTw value within an ROI was recorded, and the values of three ROIs were averaged for each patient (*Figures 2,3*).

For the ADC measurement, the two radiologists mentioned above used MITK to depict ROIs along tumor contour in consecutive DWI with b value of 1,000 s/mm^2, covering the whole lesion and also excluding visible necrosis, cysts, and vessels. The ROIs were copied to ADC maps, and the mean ADC value of the whole tumor volume was generated and recorded for statistical analysis (*Figures 2,3*).

Pathological evaluation

In this retrospective study, *KRAS* mutations at codon 12, codon 13 (exon 2), and codon 61 (exon 3) were examined by quantitative polymerase chain reaction (qPCR) using the high-resolution melting (HRM) curve analysis in 17 patients. A total of 17 cases underwent *KRAS* (exon 2) examination by PCR using the amplification refractory mutation system (ARMS) method. The ARMS method was also used in 21 cases to test *KRAS* (exons 2, 3, and 4) mutation by PCR.

Statistical analysis

Statistical analyses were performed using MedCalc Statistical Software (MedCalc, Ostend, Belgium) and SPSS R24.0.0.0 (IBM Corp., Armonk, NY, USA).

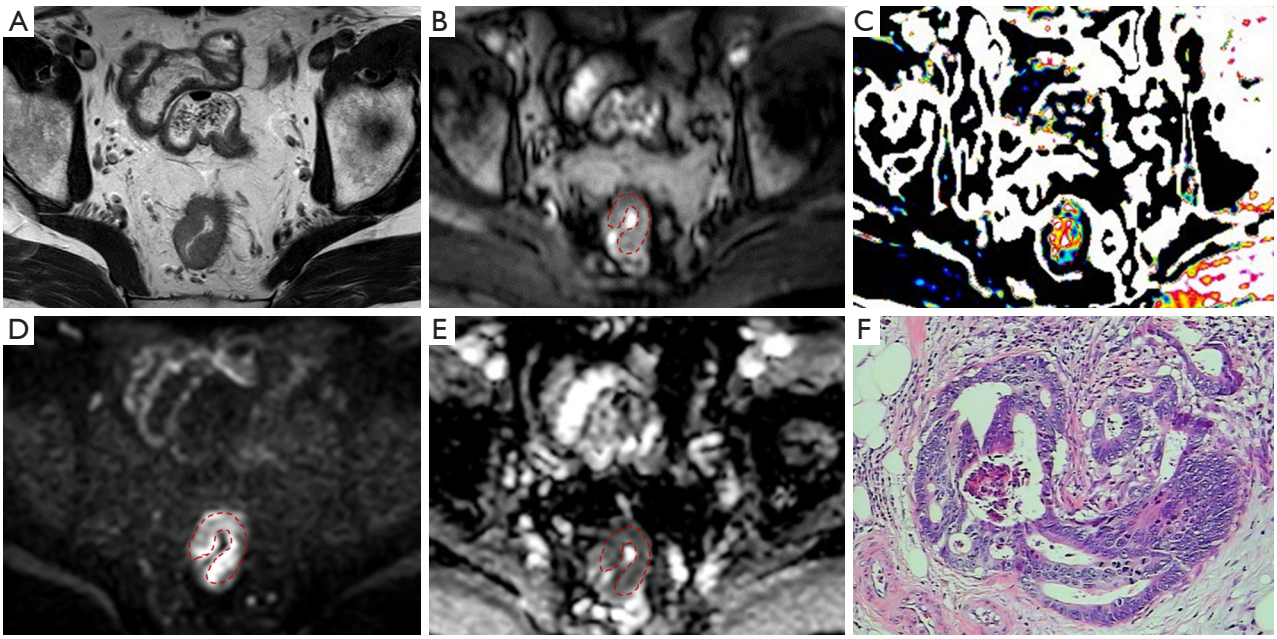

Figure 2 A 67-year-old man with *KRAS*-mutant rectal tumor. The dotted line shows the tumor contour. (A) T2WI; (B) the representative image of Z-spectrum series; (C) APTw image, the mean APTw value is 4.1%; (D) DWI with *b* value of 1,000 s/mm^2; (E) ADC map, the mean ADC is 1.04×10^{-3} mm^2/s; (F) pathological HE staining image (×40). *KRAS*, Kirsten rat sarcoma; T2WI, T2-weighted imaging; APTw, amide proton transfer-weighted; DWI, diffusion-weighted imaging; ADC, apparent diffusion coefficient; HE, hematoxylin and eosin.

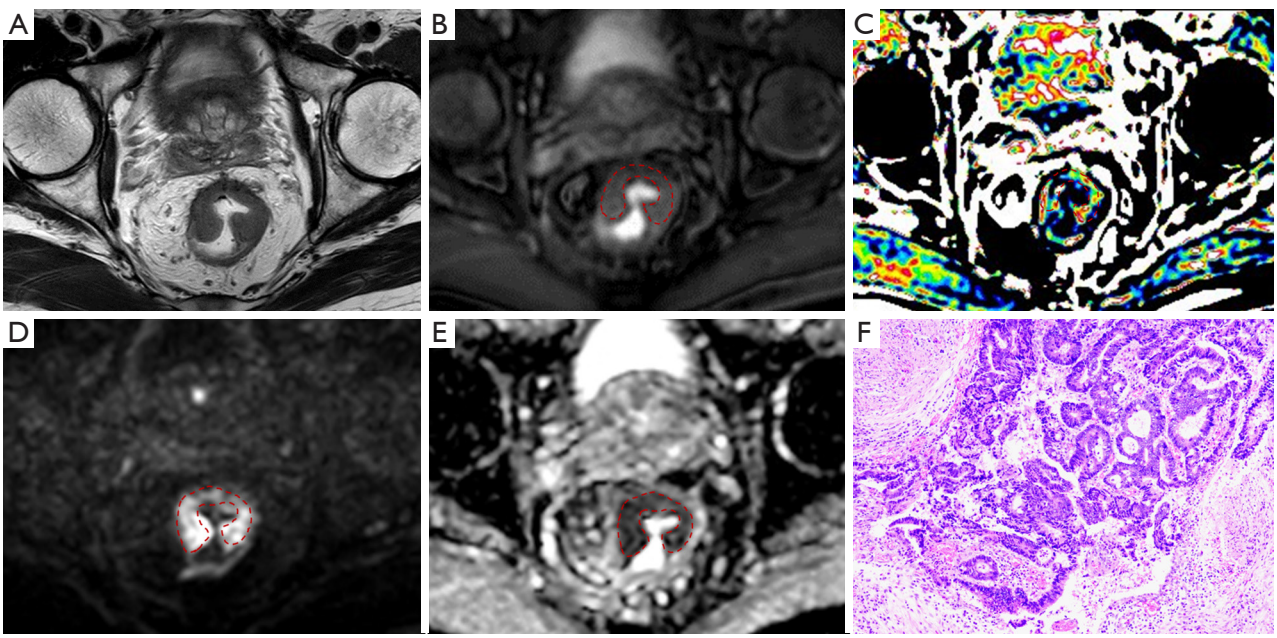

Figure 3 A 57-year-old woman with *KRAS*-WT rectal tumor. The dotted line shows the tumor contour. (A) T2WI; (B) the representative image of Z-spectrum series; (C) APTw image, the mean APTw value is 2.0%; (D) DWI with *b* value of 1,000 s/mm^2; (E) ADC map, the mean ADC value is 0.97×10^{-3} mm^2/s; (F) pathological HE staining image (×40). *KRAS*, Kirsten rat sarcoma; WT, wild type; T2WI, T2-weighted imaging; APTw, amide proton transfer-weighted; DWI, diffusion-weighted imaging; ADC, apparent diffusion coefficient; HE, hematoxylin and eosin.

Table 2 Clinical characteristics and pathological features of 55 patients

Patient characteristics	Number of cases	Number of *KRAS* cases		P value
		Mutant (n=21)	Wild type (n=34)	
Gender				0.064
Male	37	11 (29.7)	26 (70.3)	
Female	18	10 (55.6)	8 (44.4)	
Tumor location (rectum)				0.788
Upper	19	7 (36.8)	12 (63.2)	
Middle	23	8 (34.8)	15 (65.2)	
Lower	13	6 (46.2)	7 (53.8)	
Pathological T category				>0.99
T1	2	1 (50.0)	1 (50.0)	
T2	10	4 (40.0)	6 (60.0)	
T3	38	14 (36.8)	24 (63.2)	
T4	5	2 (40.0)	3 (60.0)	
Pathological N category				0.800
Negative	30	11 (36.7)	19 (63.3)	
Positive	25	10 (40.0)	15 (60.0)	
Histological grade				0.626
Well differentiated	1	0 (0.0)	1 (100.0)	
Moderately differentiated	53	20 (37.7)	33 (62.3)	
Poorly differentiated	1	1 (100.0)	0 (0.0)	

Data are presented as n or n (%). *KRAS*, Kirsten rat sarcoma.

Interobserver agreement on APTw and ADC values for two independent raters was assessed by calculating the intraclass correlation coefficient (ICC) respectively. Bland-Altman plots were also constructed, and limits of agreement (LoAs) were estimated from the plots.

The Shapiro-Wilk test was used to test the normality of APTw and ADC values. Normally distributed data were reported as the means ± standard deviations (SDs) and analyzed using the Student's *t*-test. Receiver operating characteristic (ROC) curves were constructed for APTw and ADC values respectively, and the area under the curve (AUC) with a 95% confidence interval (CI) was calculated. Cutoff values were determined to distinguish *KRAS*-mutant tumors from WT tumors according to the maximum Youden index. A P value below 0.05 with two-tailed test indicated statistical significance.

Results

Patients and pathological findings

This study consisted of 55 patients, including 37 males and 18 females. The average age of these patients was 60.02 years old. Of these 55 patients, 23 had tumors located in the middle rectum, 53 had tumors of moderate histologic grade, and 38 had tumors of pathological T3 stage. Nodal involvement was observed in 25 patients. *KRAS* mutation occurring in exon 2 was found in 21 rectal tumors. Patient characteristics are summarized in *Table 2*.

Interobserver agreement on APTw and ADC values

The ICCs of two independent raters were 0.937 (95% CI, 0.914–0.953) and 0.976 (95% CI, 0.959–0.986) for APTw

Table 3 Interobserver agreement of measurement between two radiologists for 55 rectal tumors

Parameters	Radiologist 1	Radiologist 2	ICC (95% CI)
APTw value (%)	2.705±1.182	2.659±1.231	0.937 (0.914–0.953)
ADC value (×10^{-3} mm^2/s)	1.156±0.130	1.146±0.125	0.976 (0.959–0.986)

Data are presented as mean ± standard deviation. ICC, intraclass correlation coefficient; CI, confidence interval; APTw, amide proton transfer-weighted; ADC, apparent diffusion coefficient.

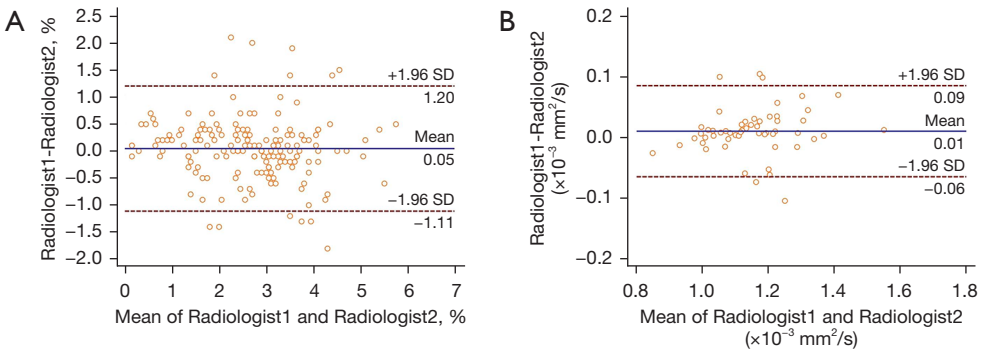

Figure 4 Bland-Altman plots of the APTw (A) and ADC (B) value measurements for 55 tumors. X-axis is the average value of two radiologists. Y-axis is the difference in values of two radiologists. SD, standard deviation; APTw, amide proton transfer-weighted; ADC, apparent diffusion coefficient.

Table 4 APTw and ADC values versus *KRAS* status in 55 rectal tumors

Parameters	*KRAS*		*t*	P value
	Mutant (n=21)	Wild type (n=34)		
APTw value (%)	3.324±0.685	2.230±0.833	4.727	<0.001
ADC value (×10^{-3} mm^2/s)	1.144±0.135	1.156±0.122	0.343	0.733

Data are presented as mean ± standard deviation. APTw, amide proton transfer-weighted; ADC, apparent diffusion coefficient; *KRAS*, Kirsten rat sarcoma.

values and ADC values, respectively, referring to excellent interobserver agreement on measurement (*Table 3*). The Bland-Altman plots showed that points tended to distribute around mean difference lines, most were within –1.96 SD to +1.96 SD of the mean (*Figure 4*). Thus, the mean measure values of two raters were used for further analyses.

Relationship between APTw values and KRAS status

KRAS-mutant tumors exhibited a higher APTw value than WT tumors in patients with rectal adenocarcinoma (3.324%±0.685% *vs.* 2.230%±0.833%, P<0.001, *Table 4*). The AUC (0.827; 95% CI, 0.701–0.916) indicated that the APTw value had moderate diagnostic value for predicting *KRAS* mutation in rectal adenocarcinoma, with a cutoff value of 2.4% (sensitivity, 95.2%; specificity, 55.9%). *Figure 5* shows the ROC curve. *Table 5* details the parameters of the ROC curve.

Relationship between ADC values and KRAS status

The ADC value was lower in the *KRAS*-mutant group than that in the WT group (*Table 4*), but it did not show a statistically significant difference between two groups (P=0.733). The ROC curve and its details are shown in *Figure 5* and *Table 5*.

Discussion

In our study, the measurement values exhibited excellent

interobserver agreement between two independent radiologists, which could be attributed to the good quality of images. We ensured good image quality by administrating raceanisodamine hydrochloride to each patient to reduce bowel peristalsis. Besides, endorectal filling by an appropriate amount of ultrasound gel could reduce gas-induced susceptibility artifacts in the rectum, which can be the problem of good B_0 homogeneity (11).

Although the ADC value of *KRAS*-mutant rectal cancer decreased in our study, there was no significant difference between the *KRAS*-mutant group and the WT group. The ADC which is obtained at *b* values of a few hundred up to 1,000 s/mm^2 mostly reflects the extracellular space (6). Oncogenic *KRAS* mutation promotes cell growth and proliferation, which tend to compress the extracellular space, resulting in a lower ADC value (6,20). Thus, the *KRAS*-mutant group exhibited a lower ADC than the WT group in our study. However, the reason for this ADC decrease resulting from cell proliferation is not straightforward and is sometimes controversial (6). Besides, the ADC does not contain all the information that can be extracted from DWI data (6). Therefore, we did not find a significant difference of ADC value between *KRAS*-mutant rectal tumors and WT tumors. Our result was consistent with the findings of some previous studies with small sample sizes (7,10). Moreover, a meta-analysis also demonstrated that ADC could not discriminate *KRAS*-mutant tumors from WT tumors in patients with rectal cancer (21).

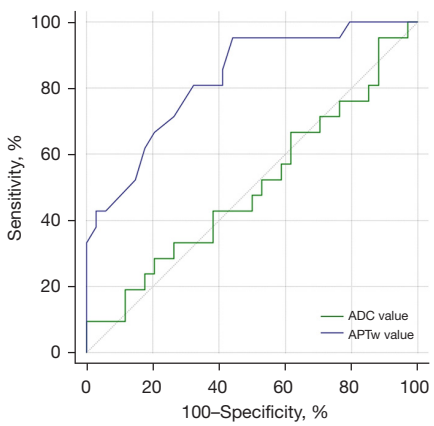

Figure 5 ROC curves for predicting *KRAS* status using APTw and ADC values. Dotted line = reference line. ADC, apparent diffusion coefficient; APTw, amide proton transfer-weighted; ROC, receiver operating characteristics; *KRAS*, Kirsten rat sarcoma.

As for the APTw value, our study demonstrated that patients with *KRAS*-mutant tumors had a higher APTw value than those with WT tumors, which meant that *KRAS*-mutant tumors showed APTw hyperintensity. APTw value is mainly determined by cellular protein content in *in vivo* tissue (11). It can also reflect intracellular pH because amide proton exchange rate is strongly dependent on pH (11). Theoretically, increased cytosolic protein content or intracellular pH can cause APTw hyperintensity in the tumor (22). The intracellular pH of solid tumors remains neutral to a little alkaline (23). Although an intracellular increase in pH would be synergistic for increased APTw value in the tumor, only a small intracellular pH increase (<0.1 unit) is often detected (22,24). Thus, the APTw hyperintensity can be mainly attribute to the increased cellular protein content in the tumor. Oncogenic *KRAS* mutation can activate several intracellular pathways to promote cell growth, proliferation, differentiation, survival, and cytokine secretion (20). All the abovementioned processes induce the increase of cellular protein content in *KRAS*-mutant rectal tumors, resulting in APTw hyperintensity. Besides, a previous study showed that the expression of vascular endothelial growth factor receptor (VEGFR)-1, VEGFR-2, and platelet-derived growth factor receptor (PDGFR)-α was significantly linked to *KRAS* codon 12 or 13 mutation in CRC (25). These signaling molecules regulate and promote tumor angiogenesis (26). Angiogenesis possibly contributes to increased protein signaling in *KRAS*-mutant rectal tumors, because the blood contains high concentrations of hemoglobin and albumin (11). Increased APTw values have also been reported in high-grade rectal tumors, more advanced stage tumors, and tumors with

Table 5 ROC analyses of APTw value and ADC value in predicting *KRAS* mutation of rectal cancer

Parameter	AUC (95% CI)	Threshold	Sensitivity	Specificity	Youden index J	P value
APTw value	0.827 (0.701–0.916)	>2.4%	95.2%	55.9%	0.5112	<0.0001
ADC value	0.503 (0.365–0.641)	≤0.931×10^{-3} mm^2/s	9.52%	100%	0.09524	0.9732

ROC, receiver operating characteristics; APTw, amide proton transfer-weighted; ADC, apparent diffusion coefficient; *KRAS*, Kirsten rat sarcoma; AUC, area under the curve; CI, confidence interval.

lymph node involvement or extramural venous invasion (17-19). In addition, a previous study demonstrated that the mean APTw value exhibited a positive correlation with p53 and Ki-67 labeling index in rectal cancer (19). Besides, APTw MRI has been used to predict the tumor response to neoadjuvant chemotherapy in patients with locally advanced rectal cancer. The low-response group had a higher mean APTw value than the high-response group in a previous study (16). APTw MRI might become a useful tool in the study of rectal cancer.

The APTw value had a moderate performance for predicting *KRAS* status in rectal non-mucinous adenocarcinoma. Its threshold for *KRAS* mutation was 2.4%, with a high sensitivity of 95.2%, but a low specificity of 55.9%. The high sensitivity meant that APTw value had a low false negative rate in *KRAS*-mutant prediction. Meanwhile, the low specificity could be explained by a previous study, which demonstrated that APTw value also increased in rectal carcinoma with p53-positive status or high expression of Ki-67 (19). Thus, if a rectal tumor shows a high APTw value, more careful pathological *KRAS* test should be performed to determine whether the mutation had actually occurred. Besides, the relationship between APTw values and prognostic factors of rectal cancer, such as *KRAS* status, p53 status, and Ki-67 expression, should be further analyzed by multivariate analysis of variance in the future.

Notably, the APT effect can be contaminated by multiple factors, such as direct water saturation (DS), semisolid magnetization transfer (MT) effects, and water longitudinal relaxation time (T_{1w}) (27). Although the MTR_{asym} analysis has been used to remove these DS and semisolid MT effects, the APTw value still includes the inherent asymmetry of the conventional MT effect and the exchange-relayed nuclear Overhauser effect (NOE) at –3.5 ppm (11). The NOE has different molecular origin from APT effect, but it is actually a positive confounding factor that can enhance the measured APTw value in tumor (28). The relationship between the NOE and *KRAS* mutation should be further analyzed in rectal cancer. Besides, T_{1w} effects contain T_{1w} recovery and T_{1w}-related saturation effects (29). These two T_{1w} effects have opposite influences on the MTR_{asym}, and can be counterbalanced by choosing appropriate saturation powers (29). T_{1w} normalization may not be necessary when appropriate sequence parameters are chosen on clinical MRI systems (29,30). An apparent exchange-dependent relaxation (AREX) method was also developed to fully remove the contamination from T_{1w}, MT, and DS effects (29). This method should be further applied in APTw MRI of rectal cancer. Additionally, liquid compartments such as cystic or necrotic structures provide artificial hyperintensity in APTw images (31). These artificial hyperintensities could be removed by fluid suppression in the neuro-oncological field (32). Although our ROIs excluded visible necrosis in rectal solid tumors, more attention should be paid to fluid suppression in further studies of body APTw MRI.

This retrospective study has several inherent limitations. First, the small number of patients included in the study may have caused bias. Patients with mucinous adenocarcinoma were excluded because mucin can make an impact on APTw value. Then, because of the technical limitation in our institution, the two-dimensional APTw MR sequence acquired only three slices of rectal tumor, resulting in underestimation of tumor heterogeneity. It was hard to accurately match slice-for-slice the APTw images and DWI images in each patient because the number of slices and slice thickness were different between these two sequences. Measurement bias might have been incurred by using the mean APTw value of three tumor slices and the mean ADC value of the whole tumor volume for statistical analyses. In addition, *KRAS* test methods in this study were variable. Although about 95% of all *KRAS* mutation types occur in exons 2 (codon 12, codon 13) (4), there were 17 patients who underwent *KRAS* mutation test at exons 2 only, which might lead to false-negative bias. Thus, we plan on performing further prospective research using a three-dimensional sequence to acquire APTw MR images of patients with rectal tumors. As shown recently, radiomics and deep learning-based T2-weighted imaging (T2WI), T2WI could evaluate *KRAS* mutation in patients with rectal carcinoma (33-35). More attention will also be paid to APTw MRI texture analyses and radiomics in rectal cancer.

Conclusions

The proposed APTw value had a moderate performance to predict *KRAS* mutation in rectal non-mucinous adenocarcinoma. APTw MRI might be a promising supplement to *KRAS* genomic analysis in rectal cancer patients. The preoperative evaluation of *KRAS* mutation could potentially be performed rapidly and noninvasively by using APTw MRI. However, the ADC derived from DWI could not determine *KRAS* mutation in rectal cancer.

Acknowledgments

We would like to express our special thanks to Doctor

Yingjie Mei from Department of Radiology, Guangdong Provincial Peoples Hospital, without whose support this paper would never have been completed. We also thank Yongzhou Xu from Philips Healthcare for her technical support.

Funding: This work was supported by the National Natural Science Foundation of China (No. 82302128), and the Scientific Research Funding Project of the Nanfang Medical Imaging Alliance (No. FS2023010010).

Footnote

Reporting Checklist: The authors have completed the STARD reporting checklist. Available at https://qims.amegroups.com/article/view/10.21037/qims-24-331/rc

Conflicts of Interest: All authors have completed the ICMJE uniform disclosure form (available at https://qims.amegroups.com/article/view/10.21037/qims-24-331/coif). The authors have no conflicts of interest to declare.

Ethical Statement: The authors are accountable for all aspects of the work in ensuring that questions related to the accuracy or integrity of any part of the work are appropriately investigated and resolved. The study was conducted in accordance with the Declaration of Helsinki (as revised in 2013). The study was approved by institutional ethics board of Zhujiang Hospital (No. 2020-KY-029-01), and individual consent for this retrospective analysis was waived.

References

1. Bray F, Laversanne M, Sung H, Ferlay J, Siegel RL, Soerjomataram I, Jemal A. Global cancer statistics 2022: GLOBOCAN estimates of incidence and mortality worldwide for 36 cancers in 185 countries. CA Cancer J Clin 2024;74:229-63.
2. Zhu G, Pei L, Xia H, Tang Q, Bi F. Role of oncogenic KRAS in the prognosis, diagnosis and treatment of colorectal cancer. Mol Cancer 2021;20:143.
3. De Mattia E, Polesel J, Mezzalira S, Palazzari E, Pollesel S, Toffoli G, Cecchin E. Predictive and Prognostic Value of Oncogene Mutations and Microsatellite Instability in Locally-Advanced Rectal Cancer Treated with Neoadjuvant Radiation-Based Therapy: A Systematic Review and Meta-Analysis. Cancers (Basel) 2023;15:1469.
4. Tan C, Du X. KRAS mutation testing in metastatic colorectal cancer. World J Gastroenterol 2012;18:5171-80.
5. Benson AB, Venook AP, Al-Hawary MM, Azad N, Chen YJ, Ciombor KK, et al. Rectal Cancer, Version 2.2022, NCCN Clinical Practice Guidelines in Oncology. J Natl Compr Canc Netw 2022;20:1139-67.
6. Le Bihan D. Apparent diffusion coefficient and beyond: what diffusion MR imaging can tell us about tissue structure. Radiology 2013;268:318-22.
7. Jo SJ, Kim SH. Association between oncogenic RAS mutation and radiologic-pathologic findings in patients with primary rectal cancer. Quant Imaging Med Surg 2019;9:238-46.
8. Xu Y, Xu Q, Sun H, Liu T, Shi K, Wang W. Could IVIM and ADC help in predicting the KRAS status in patients with rectal cancer? Eur Radiol 2018;28:3059-65.
9. Cui Y, Cui X, Yang X, Zhuo Z, Du X, Xin L, Yang Z, Cheng X. Diffusion kurtosis imaging-derived histogram metrics for prediction of KRAS mutation in rectal adenocarcinoma: Preliminary findings. J Magn Reson Imaging 2019;50:930-9.
10. Tang C, Lu G, Xu J, Kuang J, Xu J, Wang P. Diffusion kurtosis imaging and MRI-detected extramural venous invasion in rectal cancer: correlation with clinicopathological prognostic factors. Abdom Radiol (NY) 2023;48:844-54.
11. Zhou J, Heo HY, Knutsson L, van Zijl PCM, Jiang S. APT-weighted MRI: Techniques, current neuro applications, and challenging issues. J Magn Reson Imaging 2019;50:347-64.
12. Wang HJ, Cai Q, Huang YP, Li MQ, Wen ZH, Lin YY, Ouyang LY, Qian L, Guo Y. Amide Proton Transfer-weighted MRI in Predicting Histologic Grade of Bladder Cancer. Radiology 2022;305:127-34.
13. Yu H, Zhu L, Wang Y, Yue X, Wang W, Sun Z, Jiang S, Chen Y, Wen Z. Amide Proton Transfer Weighted MR Imaging for Predicting Meningioma Stiffness: A Feasibility Study. J Magn Reson Imaging 2023;57:1071-8.

14. Li S, Liu J, Zhang Z, Wang W, Lu H, Lin L, Zhang Y, Cheng J. Added-value of 3D amide proton transfer MRI in assessing prognostic factors of cervical cancer: a comparative study with multiple model diffusion-weighted imaging. Quant Imaging Med Surg 2023;13:8157-72.
15. Wáng YXJ, Dou W, Shen Z, Zhang Y. An update on liver chemical exchange saturation transfer imaging with a focus on clinical translation. Quant Imaging Med Surg 2023;13:4057-76.
16. Nishie A, Asayama Y, Ishigami K, Ushijima Y, Takayama Y, Okamoto D, Fujita N, Tsurumaru D, Togao O, Sagiyama K, Manabe T, Oki E, Kubo Y, Hida T, Hirahashi-Fujiwara M, Keupp J, Honda H. Amide proton transfer imaging to predict tumor response to neoadjuvant chemotherapy in locally advanced rectal cancer. J Gastroenterol Hepatol 2019;34:140-6.
17. Nishie A, Takayama Y, Asayama Y, Ishigami K, Ushijima Y, Okamoto D, Fujita N, Tsurumaru D, Togao O, Manabe T, Oki E, Kubo Y, Hida T, Hirahashi-Fujiwara M, Keupp J, Honda H. Amide proton transfer imaging can predict tumor grade in rectal cancer. Magn Reson Imaging 2018;51:96-103.
18. Chen W, Li L, Yan Z, Hu S, Feng J, Liu G, Liu B, Liu X. Three-dimension amide proton transfer MRI of rectal adenocarcinoma: correlation with pathologic prognostic factors and comparison with diffusion kurtosis imaging. Eur Radiol 2021;31:3286-96.
19. Li L, Chen W, Yan Z, Feng J, Hu S, Liu B, Liu X. Comparative Analysis of Amide Proton Transfer MRI and Diffusion-Weighted Imaging in Assessing p53 and Ki-67 Expression of Rectal Adenocarcinoma. J Magn Reson Imaging 2020;52:1487-96.
20. Lavoie H, Therrien M. Regulation of RAF protein kinases in ERK signalling. Nat Rev Mol Cell Biol 2015;16:281-98.
21. Surov A, Pech M, Powerski M, Woidacki K, Wienke A. Pretreatment Apparent Diffusion Coefficient Cannot Predict Histopathological Features and Response to Neoadjuvant Radiochemotherapy in Rectal Cancer: A Meta-Analysis. Dig Dis 2022;40:33-49.
22. Zhou J, Wilson DA, Sun PZ, Klaus JA, Van Zijl PC. Quantitative description of proton exchange processes between water and endogenous and exogenous agents for WEX, CEST, and APT experiments. Magn Reson Med 2004;51:945-52.
23. Griffiths JR. Are cancer cells acidic? Br J Cancer 1991;64:425-7.
24. Lee DH, Heo HY, Zhang K, Zhang Y, Jiang S, Zhao X, Zhou J. Quantitative assessment of the effects of water proton concentration and water T(1) changes on amide proton transfer (APT) and nuclear overhauser enhancement (NOE) MRI: The origin of the APT imaging signal in brain tumor. Magn Reson Med 2017;77:855-63.
25. Schimanski CC, Zimmermann T, Schmidtmann I, Gockel I, Lang H, Galle PR, Moehler M, Berger MR. K-ras mutation status correlates with the expression of VEGFR1, VEGFR2, and PDGFRalpha in colorectal cancer. Int J Colorectal Dis 2010;25:181-6.
26. Ferrara N, Kerbel RS. Angiogenesis as a therapeutic target. Nature 2005;438:967-74.
27. Zu Z. Towards the complex dependence of MTR(asym) on T(1w) in amide proton transfer (APT) imaging. NMR Biomed 2018;31:e3934.
28. Zhou J, Hong X, Zhao X, Gao JH, Yuan J. APT-weighted and NOE-weighted image contrasts in glioma with different RF saturation powers based on magnetization transfer ratio asymmetry analyses. Magn Reson Med 2013;70:320-7.
29. Cui J, Zhao Y, Sun C, Xu J, Zu Z. Evaluation of contributors to amide proton transfer-weighted imaging and nuclear Overhauser enhancement-weighted imaging contrast in tumors at a high magnetic field. Magn Reson Med 2023;90:596-614.
30. Heo HY, Lee DH, Zhang Y, Zhao X, Jiang S, Chen M, Zhou J. Insight into the quantitative metrics of chemical exchange saturation transfer (CEST) imaging. Magn Reson Med 2017;77:1853-65.
31. Zhou J, Zaiss M, Knutsson L, Sun PZ, Ahn SS, Aime S, et al. Review and consensus recommendations on clinical APT-weighted imaging approaches at 3T: Application to brain tumors. Magn Reson Med 2022;88:546-74.
32. Schüre JR, Casagranda S, Sedykh M, Liebig P, Papageorgakis C, Mancini L, Bisdas S, Nichelli L, Pinter N, Mechtler L, Jafari R, Boddaert N, Dangouloff-Ros V, Poujol J, Schmidt M, Doerfler A, Zaiss M. Fluid suppression in amide proton transfer-weighted (APTw) CEST imaging: New theoretical insights and clinical benefits. Magn Reson Med 2024;91:1354-67.
33. Xiang Y, Li S, Song M, Wang H, Hu K, Wang F, Wang Z, Niu Z, Liu J, Cai Y, Li Y, Zhu X, Geng J, Zhang Y, Teng H, Wang W. KRAS status predicted by pretreatment MRI radiomics was associated with lung metastasis in locally advanced rectal cancer patients. BMC Med Imaging 2023;23:210.
34. Liu H, Yin H, Li J, Dong X, Zheng H, Zhang T, Yin Q,

Zhang Z, Lu M, Zhang H, Wang D. A Deep Learning Model Based on MRI and Clinical Factors Facilitates Noninvasive Evaluation of KRAS Mutation in Rectal Cancer. J Magn Reson Imaging 2022;56:1659-68.

35. Song K, Zhao Z, Ma Y, Wang J, Wu W, Qiang Y, Zhao J, Chaudhary S. A multitask dual-stream attention network for the identification of KRAS mutation in colorectal cancer. Med Phys 2022;49:254-70.

Cite this article as: Yang X, Qiu Q, Lu W, Chen B, Zhao M, Liang W, Wen Z. Prediction of Kirsten rat sarcoma (*KRAS*) mutation in rectal cancer with amide proton transfer-weighted magnetic resonance imaging. Quant Imaging Med Surg 2024;14(10):7061-7072. doi: 10.21037/qims-24-331